J. exp. Biol. **107**, 245–275 (1983)
Printed in Great Britain © *The Company of Biologists Limited 1983*

THE MECHANICS OF THE PREDATORY STRIKE OF THE PRAYING MANTID *HEIRODULA MEMBRANACEA*

BY P. T. A. GRAY* AND P. J. MILL

Department of Pure and Applied Zoology, University of Leeds, Leeds LS2 9JT, U.K.

(*Received 19 January 1983–Accepted 3 June 1983*)

SUMMARY

1. The mechanics of the predatory strike of *Heirodula membranacea* (Burm.) have been studied using high speed ciné, electrophysiological and anatomical techniques.

2. Calculations of the muscle output required to produce the strike suggest that muscle performance generally lies within the range observed elsewhere and that no specializations for prior energy storage, as are found in some other rapid insect movements, are necessary.

3. This view is supported by simultaneous EMG and ciné studies showing no significant delay between the onset of EMG activity and the onset of stress development required by the direct action model.

4. The apodemes of a number of forelimb muscles are found to have complex two-point suspensions; these have a significant role in determining the moment-arm/joint-angle relationships of the muscles.

5. The parallel-fibred part of the tibial flexor muscle has a high strain rate, $17{\cdot}5\ s^{-1}$, at 27–30 °C. This is the fastest recorded strain rate for an insect muscle, and approaches the fastest strain rates of mammalian muscles operating at 37 °C.

INTRODUCTION

The predatory strike of praying mantids is both rapid and precise. Durations of 30–70 ms have been reported (Mittlestaedt, 1954; Roeder, 1959; Maldonado, Levin & Barros-Pita, 1967), though more recent work on three different species suggests that there is a fast phase of 50–70 ms preceded by a slow variable phase lasting about 100 ms (Copeland, 1975; Corrette, 1980; Gray, 1981). When preying on flies, unrestrained mantids achieve successful captures in 85–90 % of strikes (Mittlestaedt, 1957; Maldonado *et al.* 1967). Furthermore, the forelimbs are exceedingly robust and are able to restrain large prey after capture, and indeed Frank (1930) observed an unidentified mantid eating a live frog larger than itself.

The strike is of interest both from the point of view of the mechanical problems involved in such a rapid action and in terms of its initiation and control by the nervous system. A central question relating to both these aspects is whether the strike occurs

* Present address: Department of Pharmacology, University College London, London WC1E 6BT, U.K.
Key words: Muscle mechanics, praying mantid, predatory strike.

Table 1. *Peak values of muscle output parameters*

Muscle	Stress ($kN\,m^{-1}$)	Strain rate (s^{-1})	Power ($W\,kg^{-1}$)	Source
Rat extensor digitorum longus (37 °C)	300	17·2		Prosser (1973)
Rat anterior tibialis (38 °C)			570	Bennet-Clark (1977)
Mouse extensor digitorum longus (37 °C)		22		Close (1972)
Dog hind leg muscles	230–260			Alexander (1974)
Pigeon flight muscles				
Peak instantaneous (estimated)			860	Pennycuick & Parker
Peak continuous			100	(1966)
Humming bird flight muscle			150 (continuous)	Weis-Fogh & Alexander (1977)
Lobster anterior remotor				
Fast division	2·5			Mendelson (1969)
Slow division	280			
Locust metathoracic tibial extensor (30 °C)	750	1·75	450	Bennet-Clark (1975)
Locust flight muscle (30 °C)	400	13	170 (continuous)	Weis-Fogh (1956), Weis-Fogh & Alexander (1977)
Cockroach coxal muscle	80			Prosser (1973)
Drosophila flight muscle			160 (continuous)	Weis-Fogh & Alexander (1977)

by direct muscle action or by a mechanism which allows muscle activation and energy storage prior to the movement.

Peak values of stress, strain rate and specific power output obtainable by a number of arthropod and vertebrate muscles are fairly well documented; some examples of these are given in Table 1. In a number of rapid arthropod 'one off' movements, instantaneous power outputs in excess of those predicted from the values for specific power output in Table 1 and muscle size have been found to be necessary. In these cases power amplification mechanisms which allow slow energy storage prior to a rapid movement have been found, for example in the jumps of the flea (Bennet-Clark & Lucey, 1967), the click beetle (Evans, 1972, 1973), the locust (Bennet-Clark, 1975) and the flea beetle (Ker, 1977) and also in the strike of the mantid shrimp (Burrows, 1969).

The work described here was carried out to determine whether any prior energy storage mechanism is involved in the strike, to compare mantid forelimb muscle performance during the strike with existing observations of muscles from other animals and to identify any structural and muscular adaptations of the forelimb relating to the strike.

MATERIALS AND METHODS

Heirodula membranacea, the praying mantid used in this study, and its culture are described by P. T. A. Gray & P. J. Mill (in preparation).

The adult females were fed either five flies three times a week, if they were breeding stock, or two flies three times a week for experimental animals. These quantities are considerably less than an adult mantid will eat if fed *ad libitum* but quite sufficient for maintaining healthy animals. The experimental animals were fed less as this results in an increase in the ease of eliciting strikes and in a greater life span (Maldonado *et al.* 1967).

Moment arms

The moment arms of the principal muscles acting about the coxal–trochanteral (C–T) and femoral–tibial (F–T) articulations were measured by pulling their apodemes with a micromanipulator calibrated to 0·01 mm. The distance moved by the apodeme was measured as the articulation was moved through a set of consecutive 15° arcs covering, as nearly as possible, its whole range of movement. Three sets of readings were taken from each preparation and three preparations were used for each moment arm.

A second method involved embedding the articulation in wax and sectioning with a scalpel to expose the attachment points of the apodemes and positions of the articulations. These were photographed and tracings were made from the prints. From these the positions of the main apodeme attachments could be defined in terms of the distance from the articulation and the angle formed between the midline of the podomere and the line joining the articulation and attachment (Figs 1, 2). From this data moment arms were calculated for 10° steps.

The moment arm of the coxal promotor (CP) was calculated using the latter method only, as the apodeme pulling technique proved impracticable (Fig. 3). The moment arm of the thoracic trochanteral extensor (TTrE) muscle about the prothoracic coxal (P–C) articulation was measured directly as the perpendicular distance between the centre of the muscle bundle and the articulation (Fig. 4). This was measured in 21 preparations fixed in Brazil 1904 fixative (Gray, 1954) at various angles covering the whole movement range of the articulation. All the moment arms were scaled to a coxa length of 18·5 mm (the distance from the proximal tip to the C–T joint) except for those of the tibia which were corrected to a femur length of 18·5 mm (the distance from the distal tip of the trochanter to the F–T articulation).

Muscle dimensions

Forelegs were fixed in Brazil 1904 with all the articulations forming right angles. The muscles were dissected out whole with their apodemes, dabbed dry on tissue and weighed. Each muscle was weighed three times, being replaced in fixative between weighings. In the case of pennate muscles ten muscle fibres, taken from all parts of the muscle, were measured under a Zeiss OPMI microscope equipped with a graticule eye-piece. For two of the legs the layer thickness (see Alexander, 1974) was measured at five to eight points on each muscle. Finally the apodeme surface area was measured with the same equipment by measuring the length and sampling the width at 10 points. The width and depth of the fibre bundles of parallel-fibred muscles were sampled at 10 points, from which cross-sectional areas were calculated assuming a rectangular cross section. Fibre lengths were measured as for the pennate muscles. The trochanteral extensor apodeme, the heaviest, was weighed in three preparations.

Its mass of about 1·5 mg compares with about 70 mg for the combined extensor muscles (Table 2). Thus the error in ignoring the apodeme mass is approximately 2 % and hence all muscle masses given include the apodeme.

The effect of fixation on muscle mass was determined by comparing the fixed mass of the femoral muscle of one leg with the total unfixed soft tissue of the femur of the contralateral leg. Soft tissue mass was determined by weighing the femur before and after removal of all soft tissues.

The cross-sectional areas (a_m) of both pennate and parallel fibred muscles were calculated using the equation

$$a_m = m_m/l_m \,.\varrho, \tag{1}$$

where m_m is the mass, l_m the fibre length and ϱ the density of the muscle. As a_m for parallel-fibred muscles was also measured directly as described above, an independent check of accuracy is possible (Table 2). For pennate muscles, a_m can also be calculated using the equation

$$a_m = a_p \sin \alpha, \tag{2}$$

where a_p is the total apodeme surface area and α is the angle of pennation.

Thus

$$\alpha = \sin^{-1}(m_m/l_m \,.\, a_p \,.\, \varrho). \tag{3}$$

α can also be calculated from

$$\alpha = \sin^{-1}(t_m/l_m), \tag{4}$$

where t_m is the layer thickness.

These two methods of calculating α hence provide an independent check of the dimensions of pennate muscles (Table 2).

As the fibres of pennate muscles exert their pull at an angle (α) to the apodeme, the effective cross-sectional area $a_{m(E)}$ acting along the apodeme axis is given by

$$a_{m(E)} = a_m \cos \alpha. \tag{5}$$

In addition, a pennate muscle fibre contracting through length x moves the apodeme only by a distance of x cos α. To allow for this effect, the values of l_m used in calculations of rates of shortening and power output are derived from

$$l_{m(E)} = l_m \cos \alpha. \tag{6}$$

Equations (5) and (6) only hold strictly if α remains constant. In this study pennation angles were measured with the muscle half extended and were assumed to remain constant. Using this assumption, errors in α should not exceed 5 ° at the extremes of movement.

Filming

Adult female mantids were copulated, starved for 3–5 days and then fixed by the prothorax in a holder, ventral side up (their normal resting position). A hardboard disc was provided for the rear four legs. Strikes were elicited by placing live flies, fixed to a pin, about 3 cm in front of the animals' eyes. At least 20 strikes in one day could

be elicited in this manner from a good preparation. Before filming, the approximate positions of the centres of mass of the limb podomeres were marked with a dot of black ink.

Films were taken at 300–1000 frames per second with a Hitachi HIMAC 16 HS camera on Ilford black and white 16 mm film. Illumination was provided by two Redhead 800 W flood lamps, reflected by mirrors to reduce the infrared content of the light. The temperature recorded by a thermometer suspended close to the experimental animal was noted immediately after turning the lights off after filming. It was between 27 and 30 °C for all films. A 100 Hz signal was fed to the time marker neon of the camera. Immediately after filming, the animals were killed and the leg that had been further from the camera, together with the prothorax, was fixed in Brazil 1904 for later measurement of muscle dimensions as described above. The leg which had been nearer to the camera was cut into its constituent podomeres, except the trochanter and femur which were left joined since they are treated as a single podomere in the mechanics calculations. The podomeres were weighed and the positions of their centres of mass checked, using the method of Alexander (1968).

Data analysis

Five strikes were selected for analysis using the following criteria: (a) no two strikes should be by the same animal, (b) the acceleration of the camera during the strike should be small enough to be neglected (less than 5 %), and (c) the film speed should be not less than 300 frames per second. Frames from films were analysed on a PCD film analyser at intervals such that the time between sample points was 2·3–3·3 ms in the fast, later part of the strike and 5–7 ms in the slow, earlier part.

Due to lack of film definition and poor camera framing there were small, unavoidable errors in the measurements of limb position from the film. When differentiated twice these errors produced an unacceptably high level of high frequency noise in the acceleration/time records which in turn resulted in noise in the calculated muscle output parameter records. To reduce the effects of this problem, acceleration was calculated using a polynomial smoothing technique over nine sample points (Lanczos, 1957). A similar problem arose in the calculation of angular velocity and for this a five-sample points smoothing technique was used (Lanczos, 1957).

Such techniques can introduce distortions, particularly where rapid changes in velocity or acceleration occur. To provide some assessment of the effect of the acceleration smoothing technique on the data, some accelerations were also calculated using

(i) the five-point acceleration smoothing technique (Lanczos, 1957) and

(ii) no smoothing, using the equation

$$\ddot{x} = \frac{x_3 - 2x_2 + x_1}{t^2},$$

where $\ddot{x} = d^2x/dt^2$ (acceleration), x_1–x_3 are three consecutive position measurements each displaced by time t from the preceding value.

A-band lengths

Fresh muscle fibres were examined under a Zeiss Nomarski optics microscope and A-band lengths measured with a micrometer eyepiece.

Apodeme cross-sectional areas

Apodemes were stripped of muscle fibres, embedded in Araldite and thick (about 0·25 mm) sections were made using a sharp razor blade. The sections were mounted on slides and projected onto graph paper using a Watkins Hilux 70 microscope. The outline was traced and the area measured. Sections were taken from the end nearest to the attachment, where the apodemes were thickest.

Frictional effects

The effects of resistive forces on the strike were determined by observing the reduction in rate of fall of a mass when the mass in falling had to extend the coxo–trochanteral articulation.

A rotational position transducer, substantially linear, was loaded with a 5 g mass, (Fig. 11A). The transducer output was stored by a Datalab DL 901 transient recorder and displayed on a Tektronix 564B oscilloscope. The acceleration of the mass was measured with and without the tip of a forelimb femur being attached by a light and effectively strainless thread to the tip of the transducer. Movement was restricted to $\pm 22{\cdot}5°$ about the horizontal, enabling the line of force of the connecting thread and of the gravitational force $\boldsymbol{g}$ to be taken as effectively tangential to the transducer arm and limb podomere.

The tip of the transducer arm or femur was held at the upper limit of movement by a length of 40 μm diameter copper wire. Cutting this wire with a pair of scissors was assumed to give instantaneous release.

Phasing of muscle activity

The phasing of muscle activity with movement was investigated using implanted paired 40 μm copper wire electrodes positioned just inside the cuticle amongst fibres of the muscles under study. Signals were amplified and stored on tape. A 100 Hz signal was recorded on the tape and fed to a time marker neon in the ciné camera which was used to take simultaneous films of strikes as previously described. The 100 Hz signal together with a single event pulse, also recorded on both film and tape, enable synchronization of the records. Full details of the methods are given by Gray (1981).

Measurement of peak tibial flexor strain rate

Strain rates in the tibial flexor muscles were measured by attaching the flexor apodeme to a 40 μm copper wire carrying a light paper flag. The wire passed over a pulley and was tensioned with 1 g. A photodiode mounted on a micromanipulator was positioned close behind the flag and a torch in front. The output of the diode was stored, after amplification with a DL401 transient recorder, and displayed on a Telequipment DM63 oscilloscope. The main leg nerve, 5, was stimulated *via* a pair of silver wire hooks. The shift in output signal from the diode and the time taken in response to the muscle contraction was measured. After each trial, the same displacement signal was reproduced by moving the diode past the flag with a calibrated micromanipulator to determine the distance moved.

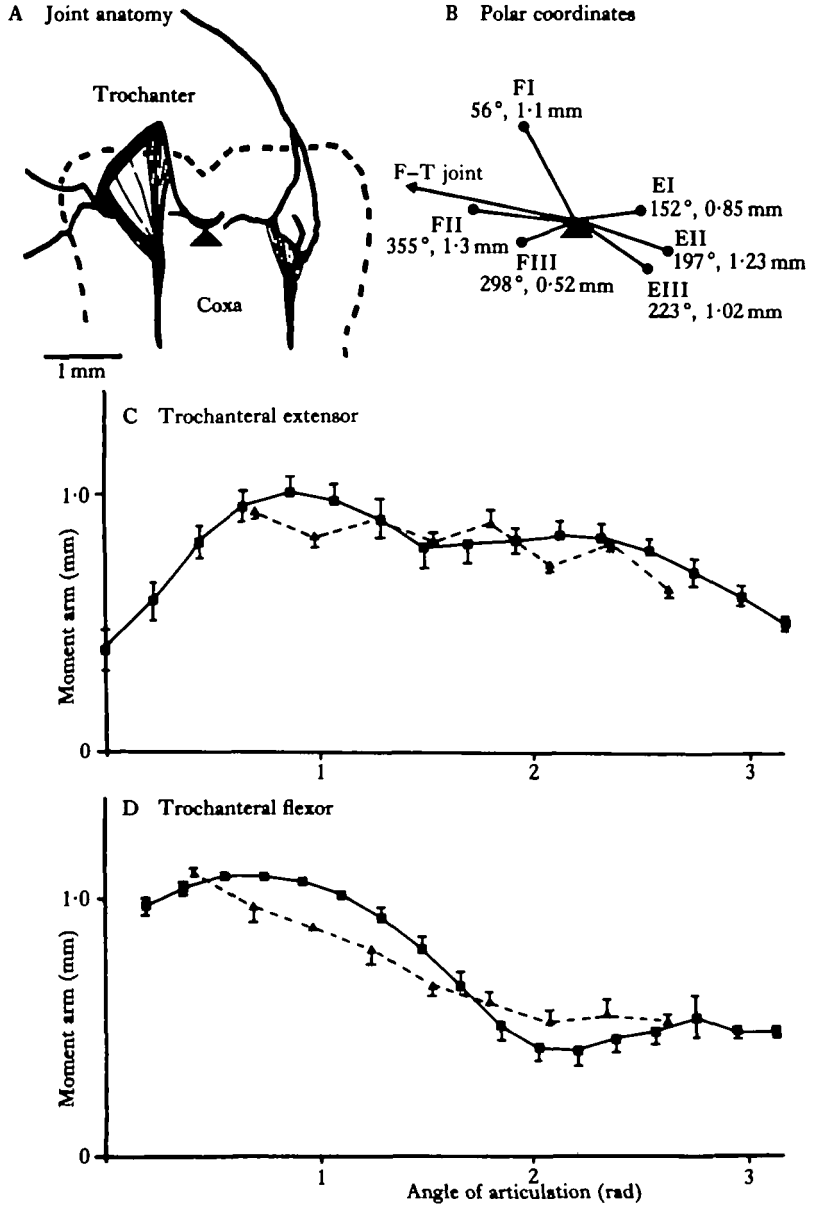

Fig. 1. Coxo–trochanteral moment arms. (A) Anatomy of the articulation and muscle attachments. Solid triangle indicates the position of the articulation. (B) Polar coordinates of the muscle attachments. EI and EII are the primary and secondary extensor attachments respectively. EIII is the position of the effective third apodeme suspension formed at the apex of the two suspensory ligaments. FI, II, III are the flexor apodeme attachments (labelled similarly). (C) Trochanteral extensor moment arms. The solid lines are calculated from the articulation geometry by the equation MA = x cos $(270°+\beta-\alpha-AA)$. The values plotted are calculated from the attachment (i.e. EI, EII or EIII) that gives the maximum MA at each point. x is the distance of the attachment from the articulation; β is the angle between the apodeme and the axis of the coxa (5° for both extensor and flexor apodemes); α is the position with respect to the line joining the coxo–trochanteral and femoro–tibial articulations; AA is the angle of articulation. The dashed lines are moment arms calculated from the apodeme pulling experiments. Errors bars are standard errors ($N = 3$). (D) Trochanteral flexor moment arms. As (C) except moment arms here calculated from the positions of the flexor apodeme attachments as: MA = x cos $(\alpha+AA-90°-\beta)$.

RESULTS

Moment arms

Figs 1 and 2 show the anatomy of the apodeme attachments and moment arms of the principal muscles operating round the C–T and F–T articulations. The suspensions of each of the four apodemes shown in these figures are formed by straplike membranes in such a way that the effective point of suspension moves as the angle of pull on the apodeme changes. Manipulation of the apodemes shows that in all four cases they behave largely as though suspended by discrete ligaments from two points. There are, in effect, three apodeme attachments in each case as over part of the range of angle of articulation the apodemes are suspended at the apex of the triangles formed by the pairs of ligaments, while over the rest of the range they are suspended directly from one or other attachment. In Figs 1 and 2 the two primary attachments have been termed FI, II (flexors) or EI, II (extensors) while the effective third attachment has been termed FIII or EIII. The geometrically calculated moment arms (the solid lines in Figs 1C, D and 2C, D) were calculated on this basis. As can be seen the fit with moment arms measured by pulling the apodemes (the dashed lines) is reasonable. In no case is the difference between the two sets of results greater than 25 % and in most cases the difference is considerably smaller than this. The moment arms calculated from measurements of dissected articulations were used in the mechanics calculations, since with this method a moment arm could be easily calculated for any angle of articulation and there was general agreement between the two methods of calculating moment arms.

For the tibial flexor apodeme the moment arm calculated with allowance made for the principal apodeme suspension only is also plotted against angle of articulation (the dotted line in Fig. 2D).

The anatomy of the P–C articulation and the coxal promotor apodeme attachment is illustrated in Fig. 3A, B. In this case the apodeme is effectively suspended at only one point, as indicated in Fig. 3C, which shows tracings from photographs taken with the apodeme held in tension at a number of different angles. Fig. 3D illustrates the moment arm of the CP (calculated by the equation shown in the legend) plotted against angle of articulation. The anatomy of the thoracic trochanteral extensor muscle (TTrE) in the region of the P–C articulation and its moment arm about that articulation (plotted against angle of articulation) are shown in Fig. 4.

Muscle dimensions

The dimensions of the principal muscles involved in the strike are given in Table 2. The values are means from the five animals used for ciné film analysis. The fibre lengths and cross-sectional areas of the pennate muscles are the true values, rather than the effective values (see Materials and Methods) which have been used for mechanical calculations. The mean standard deviation of the fibre length measurements is given as a measure of the variation in fibre length within each muscle.

The values for pennation angle for the pennate muscles, calculated by two different methods, and of measured and calculated weight for the parallel-fibred muscles, provide an indication of the accuracy of the measuring techniques used.

The effects of fixation upon muscle weights were investigated by comparing total

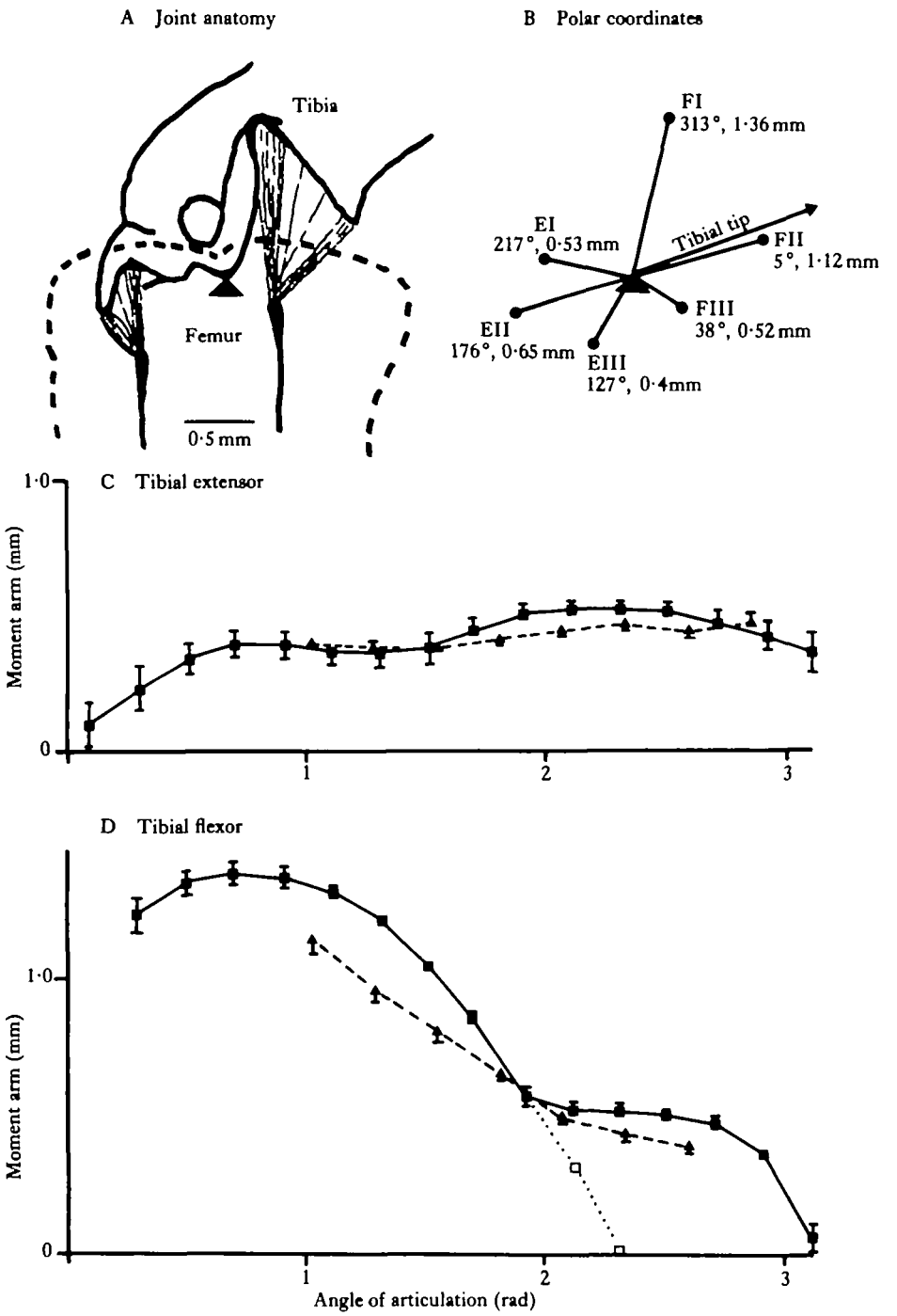

Fig. 2. Femoro–tibial moment arms. (A) Anatomy of the articulation and muscle attachments. (B) Polar coordinates of the muscle attachments labelled as in the legend to Fig. 1. (C) Tibial extensor moment arms. Solid lines calculated as in Fig. 1C. In this case β is 0° for both extensor and flexor apodemes. Dashed lines are from apodeme pulling experiments. Error bars are standard errors ($N = 3$). (D) Tibial flexor moment arms. Calculated as in Fig. 1D. The dotted line and open squares show the moment arm assuming that only FI was functional.

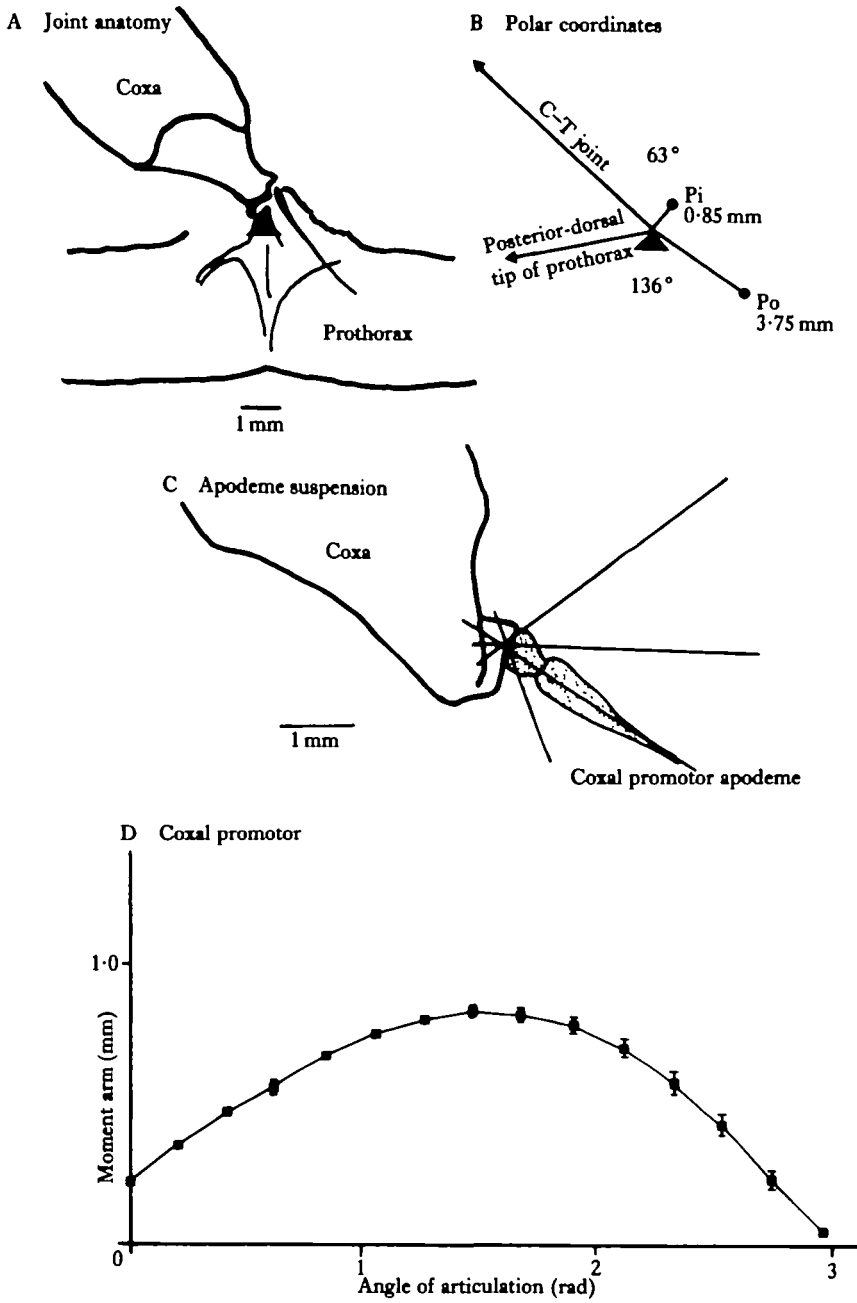

Fig. 3. Coxal promotor moment arm. (A) Prothoracic–coxal articulation anatomy. (B) Polar co-ordinates of the muscle attachments. Pi is the insertion of the muscle on the coxa, Po is the origin of the muscle in the prothorax. (C) Apodeme attachment. Superimposed traces from photographs showing that the apodeme effectively has a single suspension. (D) Moment arms. These were calculated as: $MA = x \cos\left[\tan^{-1}\left(\frac{x - y\cos\theta}{y\sin\theta}\right)\right]$, where $\theta = 360 - (\alpha+\beta) - JA$; x = distance of Pi from articulation; y = distance of Po from articulation; α = position angle of Pi with respect to the line joining the prothoracic–coxal and coxo–trochanteral articulations; β = position angle of Po with respect to the line joining the dorsal posterior tip of the prothorax and the prothoracic–coxal articulation; AA = angle of articulation. Vertical bars are standard errors ($N = 3$).

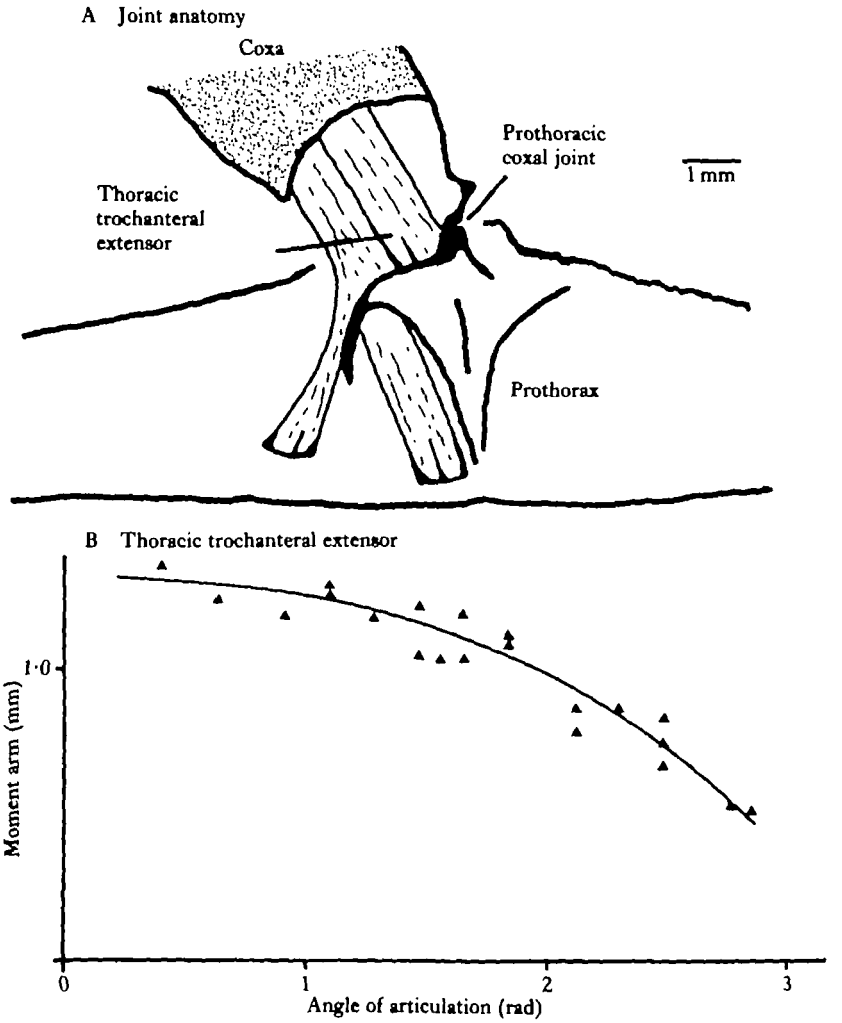

Fig. 4. Thoracic trochanteral extensor arm about the prothoracic coxal joint. (A) Joint anatomy. (B) Moment arms measured as the distance between the prothoracic–coxal articulation and the mid-point of the muscle bundle from 21 specimens of forelimbs fixed at different angles of articulation. The line is drawn by eye.

femoral unfixed soft tissue weight with the fixed weight of the femoral muscles. For four pairs of legs the mean difference was 21·3 ± 1·8 mg (S.E.M.), and the mean total fixed muscle weight was 68·5 mg. It is hard to assess what proportion of the soft tissue weight is made up of nerve trunks, trachea, haemolymph and other non-muscular tissues but visual examination suggests it is larger than the tibial extensor (approximately 10 mg). Hence measurement of fixed muscle weights should underestimate fresh muscle weights by less than 15 %.

Mechanics theory

The strike is taken as occurring in the plane of Fig. 5; moments perpendicular to this are assumed to be negligible. The trochantero–femoral (T–F) articulation has no

Table 2. *Muscle dimensions*

Muscle	l_m (mm)	S_l	α_1 (degrees)	α_2 (degrees)	a_m (mm^2)	m_m (mg)	m_m calc (mg)
CP	3·4	0·87	–	–	3·6	12·1	12·2
TTrE	10·4	1·04	–	–	1·5	15·2	16·3
CTrE	4·1	0·91	17·8	20·3*	3·5	14·4	–
TiE	4·0	0·34	18·1	19·3	2·6	10·2	–
TiF_{PAR}	10·2	0·96	–	–	2·9	29·2	29·0
TiF_{PEN}	4·2	0·94	18·1	16·8	7·0	29·3	–

* A large proportion of the fibres of CTrE are curved. Hence when calculating α_2 straight fibres were selected and t_m and l_m were measured at their tips. This weights the distribution since straight fibres tend to be at the distal end of the muscle where the fibres are shorter than average and where the pennation angle is apparently larger. The figure for α_2 for CTrE is, therefore, likely to be an overestimate of the true pennation angle.

Abbreviations: l_m, fibre lengths; S_l, mean standard deviation of fibre length for five samples of 10; α_1, α_2, pennation angles (defined above); a_m, muscle area (cross-sectional); m_m, muscle mass.

α_1 is calculated using equation 3, α_2 using equation 4.

freedom of movement in this plane, enabling the trochanter to be treated as part of the femur. The tarsus has been ignored as it is not involved in the strike and is very light (less than 2% femur mass). Hence the forelimb can be represented as in Fig. 5 for description of strike mechanics.

Each podomere has a mass m_j (where the subscript j is the podomere number). As the strike is taken as occurring in two dimensions, only the accelerations in this plane ($\ddot{x}$, $\ddot{y}$ and $\ddot{\theta}$) need to be considered. These accelerations, their associated inertial forces and the gravitational force have been drawn in Fig. 5 for podomere 2 (the femur).

Let x_j, y_j be the coordinates of the centre of mass of podomere j. Then, if the podomere mass (m_j) moves with accelerations $\ddot{x}_j$ and $\ddot{y}_j$, the inertial moment about a point x_o, y_o is

$$(y_j - y_o)\ddot{x}_j m_j - (x_j - x_o)\ddot{y}_j m_j . \tag{7}$$

Allowing for gravitational forces and the rotational couple acting around the centre of mass this becomes

$$(y_j - y_o)\ddot{x}_j m_j - (x_j - x_o)\,(\ddot{y}_j + g)m_j - I_j\ddot{\theta}_j , \tag{8}$$

where I_j is the moment of inertia of podomere j.

If frictional forces are assumed to be negligible and no other external forces act on the leg the moment of the net muscle force T_L about the articulation L must be equal and opposite to the sum of the moments about that articulation of the inertial forces acting on all leg podomeres distal to it.

Hence

$$T_L = \sum_{j=L}^{3} \{m_j[(x_j - x_L)\,(\ddot{y}_j + g) - (y_j - y_L)\ddot{x}_j] + I_j\theta_j\}, \tag{9}$$

where x_L, y_L are the coordinates of joint L.

If the torque about an articulation is produced by a parallel-fibred muscle of cross-sectional area a_m and fibre length L_m working through a moment arm x_m, then

$$\text{muscle stress } (\sigma) = \frac{T}{x_m \cdot a_m}. \tag{10}$$

If the articulation rotates with angular velocity, then

$$\text{strain rate } (v_L) = \frac{\omega \cdot x_m}{L_m}. \tag{11}$$

The power required to produce this moment is

$$T.\omega. \tag{12}$$

Expressed as power per unit mass muscle (P_m) this becomes

$$P_m = \frac{T \cdot \omega}{V \cdot \varrho}, \text{ (where V is the muscle volume)} \tag{13}$$

$$= \frac{\sigma v_L}{\varrho}. \tag{14}$$

ϱ was taken as 1000 kg m^{-3}. Mendez & Keys (1960) found ϱ of mammalian muscle to be 1060 kg m^{-3}.

Where a pair of antagonistic muscles act about an articulation the equations above can be solved unambiguously, provided that it is assumed that the antagonists are not simultaneously active. Such a simple case does not exist at any of the articulations considered in the mantid forelimb, as is shown in the diagram of the foreleg muscles in Fig. 6. When more than one muscle can contribute to the torque about an articulation assumptions must be made as to the relative contribution of each muscle to the net torque.

The assumptions made in dealing with the mantid strike are as follows. The femoro–tibial (F–T) articulation is operated by three muscles: the tibial extensor (TiE), the pennate tibial flexor (TiF_{PEN}) and the parallel-fibred tibial flexor (TiF_{PAR}), (Fig. 6) (P. T. A. Gray & P. J. Mill, in preparation). The two flexor muscles have

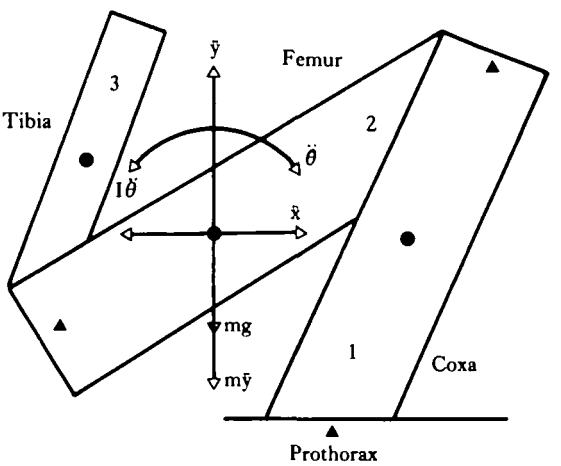

Fig. 5. Simplified diagram of a forelimb showing how the torque about the limb joints was calculated. The inertial and gravitational forces acting have been drawn in for podomere 2 (the femur). The torque about joint L (T_L) was calculated as $T_L = \sum_{j=L}^{3} \{m_j[(x_j - x_L)(\ddot{y}_j + g) - (y_j - y_L)\ddot{x}_j] + I_j\ddot{\theta}_j\}$.

been treated as if each generated the total flexor torque alone. The coxo–trochanteral (C–T) articulation is also operated by three muscles: the trochanteral flexor (TrF) a pennate extensor – the coxal trochanteral extensor, (CTrE) – and a parallel-fibred thoracic trochanteral extensor (TTrE). The small accessory extensor and flexor muscles are ignored and the four parts of the TTrE (the pleural, anterior tergal, intermediate tergal and the posterior tergal trochanteral extensors) are treated as one (Fig. 6). The latter assumption is reasonable as the fibre lengths of the four parts are very similar and they form a tight bundle until after passing proximal to the

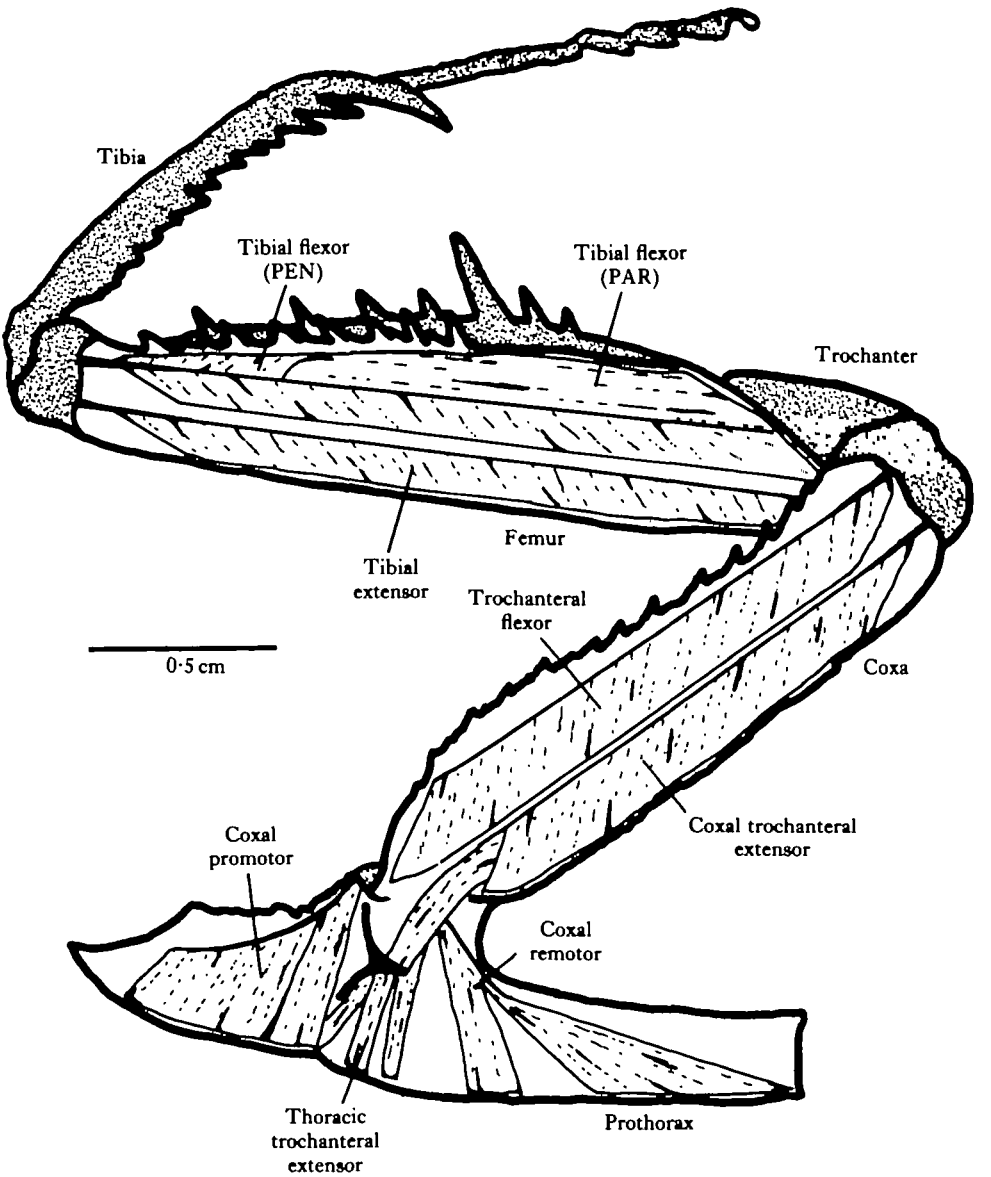

Fig. 6. The muscular anatomy of the mantid forelimb, showing the principal muscles that are involved in the predatory strike and discussed in the text. The muscles of the trochanteral/femoral and tibial/tarsal articulations are not illustrated as they play no major role in the strike.

prothoracic–coxal (P–C) articulation. Since the parallel-fibred extensor crosses this latter articulation as well as the C–T articulation, some estimation of the relative roles of CTrE and TTrE in generating the extensor torque is possible. TTrE has a remotor moment arm about the P–C articulation. Hence, if all remotor torque about the latter articulation is produced by TTrE and if its antagonist about that articulation, the coxal promotor (CP) (Fig. 6), is never active simultaneously, then the relative contributions of TTrE and CTrE to the trochanteral extensor torque can be calculated. Thus, if $T_{P-C(REM)}$ is the remotor torque about the P–C articulation and $T_{C-T(TOT)}$ is the extensor torque about the C–T articulation and $x_{m(P-C)}$ and $x_{m(C-T)}$ are the moment arms of the TTrE about the P–C and C–T articulations respectively, then the trochanteral extensor torque generated by CTrE is given by

$$T_{C-T(PEN)} = T_{C-T(TOT)} - T_{P-C(REM)} \frac{x_{m(C-T)}}{x_{m(P-C)}}. \tag{15}$$

An alternative assumption was used to determine the contributions of the leg muscles to the extensor torque about the C–T articulation in some cases. W was taken as the maximum instantaneous specific power output available from the mantid leg muscles. Where the calculated power output of CTrE exceeded this figure the following recalculation was carried out:

$$\sigma = \frac{W \cdot \varrho}{v_L} \qquad \text{(from equation 14).} \tag{16}$$

Therefore

$$T_{C-T(PEN)} = W.\ \varrho.\ a_m x_m / v_L, \tag{17}$$

where a_m, x_m, v_L and ϱ are all parameters of CTrE. Therefore

$$T_{P-C(REM)} = T_{C-T(TOT)} - W \cdot \varrho \cdot a_m x_m / v_L \frac{x_{m(P-C)}}{x_{m(C-T)}}. \tag{18}$$

This results in $T_{P-C(REM)}$ being greater than $T_{P-C(TOT)}$, the net torque about the P–C torque, and hence a promotion torque

$$T_{P-C(PROM)} = T_{P-C(REM)} - T_{P-C(TOT)} \tag{19}$$

must be generated by CP to balance the torques about this articulation. CP consists of two muscles, the pleural and tergal coxal promotors, which are treated here as a single muscle.

No calculations have been made for the mechanical behaviour of TrF or CR as these muscles are not involved in the extension phase of the leg, and hence should not be limiting factors in the speed of the strike.

Calculated results

Fig. 7 shows forelimb articulation movements during a typical strike together with calculated torques acting about the articulations for the same strike. In contrast to the relatively slow onset of movement shown in the angle of articulation plots, a clearly defined onset of torque, corresponding to the later stages of the strike, is seen. The

length of this phase until the prey is trapped between femur and tibia is about 40 ms for the strike illustrated. The arrows (a, b) show the times taken as the start (first notable deflection of the torque/time curve) and end (from the angle of articulation plots and film) of this phase. This indicates that the torques required for the earlier slow extensions of the leg articulations are small enough to be indistinguishable from the postural torques.

Figs 8 and 9 show plots of strain rate, stress and power for the muscles treated taken from the analysis of the same strike from which the plots in Fig. 7 were taken. The negative values of stress, which only occur for CTrE, are a result of the assumptions made in their calculation. The assumption that all remotor torque at the P–C articulation was generated by TTrE was made in order to assess the likely maximum contribution of this muscle to the trochanteral extensor torque. TTrE has a remotor moment arm about the P–C articulation, and thus, if it is involved in extension of the trochanter, this must result in generation of remotor torque about the P–C articulation. That this muscle, which amounts to about half the total mass of trochanteral extensor muscle, should be involved in the rapid trochanteral extension which occurs during the strike seems extremely likely. In addition, Fig. 7 shows that the peak of P–C remotor torque closely follows that of C–T extensor torque (and then decays more slowly). Hence it is reasonable to assume that the P–C remotor torque is generated by TTrE during the period when there is high extensor torque.

Using this assumption, the problem arises in the period when high P–C remotor torque continues after cessation of C–T extensor torque [that this latter occurs is not surprising as the coxal remotor (CR) would be expected to be involved in slowing the forward motion of the leg at the end of the strike, in addition to there being recoil effects due to hitting the prey]. In this situation the assumption that all remotor torque is due to TTrE activity is clearly false and leads to high negative values for CTrE stress when the effects of the two muscles are balanced about the C–T articulation. This effect occurs late in the strike, after peak C–T extensor torque has passed (marked by the arrow in Fig. 9).

Mean values of maximum strain rate, stress and specific power for each muscle for the five strikes studied are given in Table 3, which also gives peak values of these parameters and strain rate and stress at maximum power for the strike from which the data in Figs 8–11 was taken (Strike 1).

Comparison of Tables 1 and 3 reveals the performance of the mantid forelimb muscles during the strike in relation to the known performance of other muscles. The stresses and power outputs developed during the strike by the tibial musculature are low in comparison with those which can be achieved by other muscles. However, the strain rates of the flexor muscles are larger.

For the short-fibred pennate muscle (TiF_{PEN}) the maximum observed value is over twice as high ($44{\cdot}7\,s^{-1}$) as the maximum observed in other muscles. The peak strain rates in the tibial flexor muscles were observed at times when the stress and power output of the muscles were low and falling rapidly (Fig. 8B). Hence the strain rates could approach the intrinsic strain rate at this time. Those for the long, parallel-fibred muscle (TiF_{PAR}) ($17{\cdot}5\,s^{-1}$) approach these values and are higher than previously recorded intrinsic strain rates for insect muscle. As the power output and torque can easily be generated by TiF_{PAR} alone it could well be responsible for the rapid phase

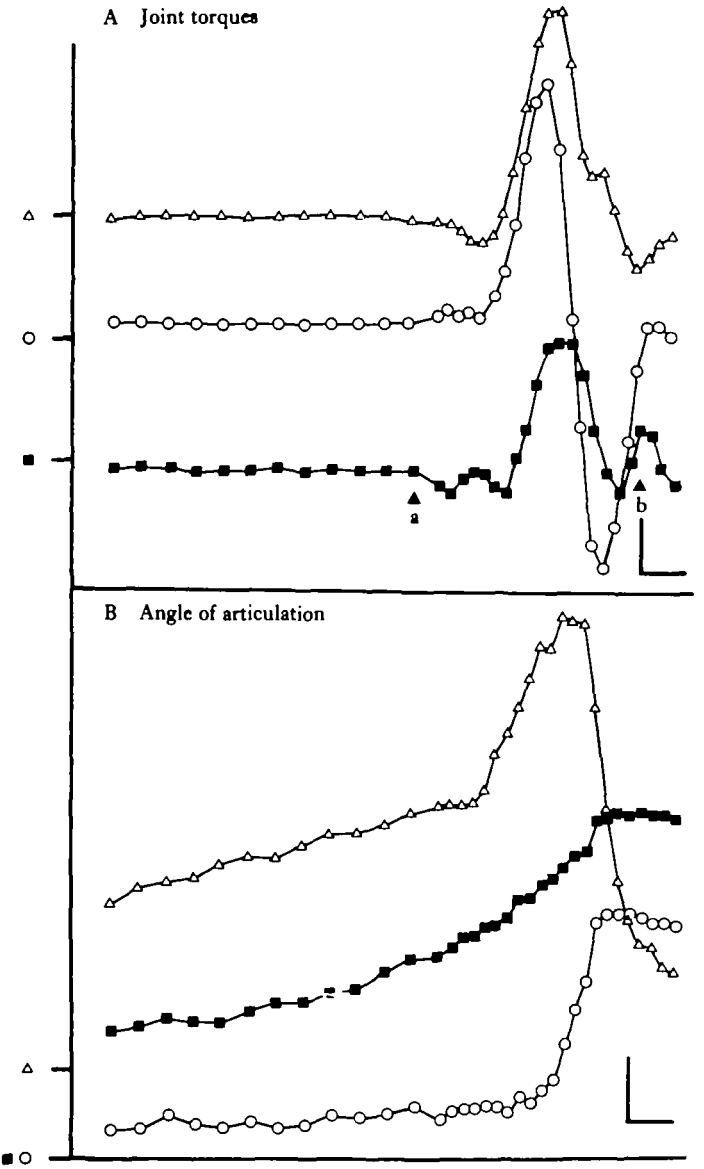

Fig. 7. (A) Torques acting about the forelimb articulations, and (B) angles of articulation during a strike (referred to as Strike 1 in the text). The arrows (a, b) show the times taken as the start and end of the final phase of the strike. The y origins of the traces are indicated by the labelled ticks on the ordinate. Solid squares, prothoracic–coxal (P–C) articulation; open circles, coxo–trochanteral (C–T) articulation; open triangles, femoro–tibial (F–T) articulation. Horizontal scale bars, (A) and (B) 10 ms; vertical scale bars, (A) 5×10^{-5} Nm P–C and C–T articulations, 5×10^{-6} Nm F–T articulation; (B) 0·25 rad.

of tibial flexion, whereas TiF_{PEN} is well-adapted for generating the high isometric torques needed to grip prey after capture.

The situation with the coxal and trochanteral musculature is more complex (Fig. 9). This is largely because of the assumptions (discussed above) made about the

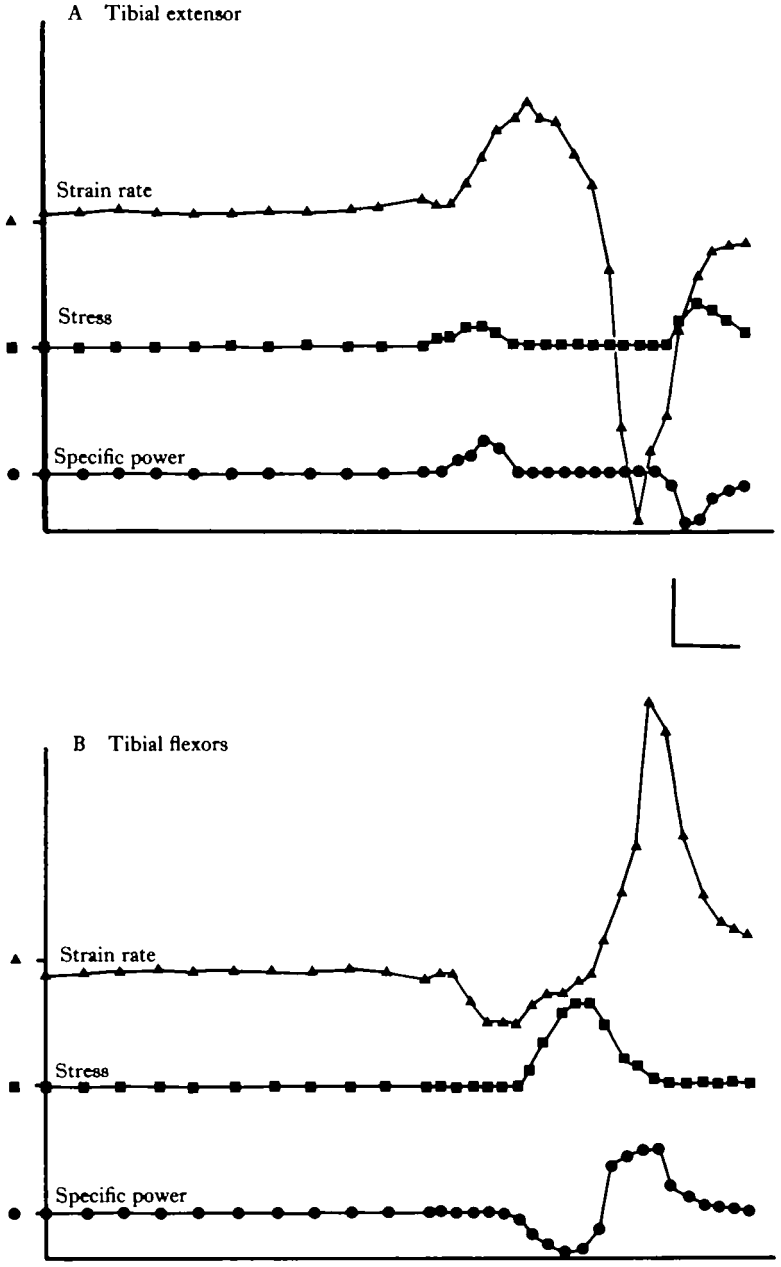

Fig. 8. Tibial musculature output parameters for Strike 1 calculated from the model described in the text. The data for (B) has been calculated for both TiF_{PAR} and TiF_{PEN} assuming in each case that the respective flexor muscle is responsible for all observed flexor torque. As the muscles share an apodeme but differ in dimension, the plots of their output are identical in shape but have different scales. Hence the vertical scale bar represents 0·625 $W g^{-1}$, 5 s^{-1}, 8·1 $kN m^{-2}$ for TiE and TiF_{PAR}. For TiF_{PEN} the vertical bar represents 0·735 $W g^{-1}$, 12·5 s^{-1}, 2·35 $kN m^{-2}$. The horizontal bar represents 10 ms.

generation of torque at the P–C and C–T articulations. However, examination of Table 3 shows that maximum stresses, strain rates and power output for CP and TTrE lie well within the range of known maxima for these parameters. In addition, the

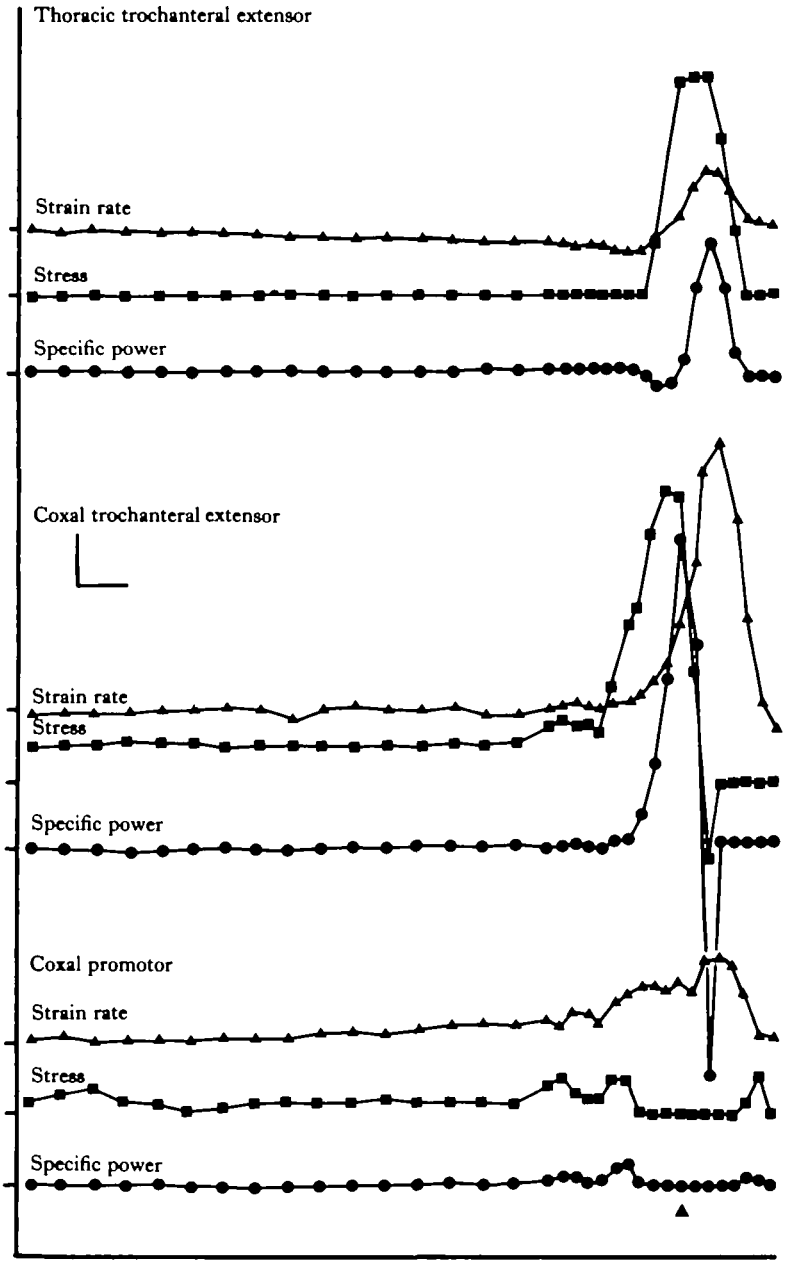

Fig. 9. Proximal musculature output parameters calculated for Strike 1. Vertical scale bar, 0·125 $W g^{-1}$, 5 s^{-1}, 16·2 kN m^{-2}. Horizontal scale bar, 10 ms. The arrow marks the time of peak trochanteral extensor torque.

values of stress and strain rates for these muscles, at the point of maximum power output, do not exceed 30 % of the maximum expected values, as would be predicted by the Hill equation.

The values for CTrE are higher, the mean peak calculated power output is 410 $W kg^{-1}$, while the peak power output for CTrE in Strike 1 exceeds 700 $W kg^{-1}$. One

Table 3. *Muscle performance during the mantid strike*

		Maximum stress ($kN\,m^{-2}$)	Maximum strain rate (s^{-1})	Maximum power ($W\,kg^{-1}$)	Stress at maximum power ($kN\,m^{-2}$)	Strain rate at maximum power (s^{-1})
Coxal promotor	(a)	10·3(2·1)	6·1(0·5)	62(7)	–	–
	(b)	11·0	5·9	55	10·9	5·0
Thoracic trochanteral extensor	(a)	63·0(0·9)	3·9(0·8)	200(40)	–	–
	(b)	66·2	4·8	320	66·2	4·8
Coxal trochanteral extensor	(a)	54·1(13·9)	14·6(2·1)	410(130)	–	–
	(b)	88·6	14·5	740	87·8	8·4
Tibial extensor	(a)	2·1(0·6)	4·5(0·8)	6(2)	–	–
	(b)	2·2	6·9	10	2·2	4·7
Tibial flexor (parallel)	(a)	9·1(0·1)	17·5(1·6)	27(5)	–	–
	(b)	10·9	20·7	22	1·0	20·7
Tibial flexor (pennate)	(a)	3·9(0·3)	44·7(4·1)	30(6)	–	–
	(b)	5·1	52·0	26	0·5	52·0

Figures in rows (a) are means for five strikes (± S.E.M.).
Figures in rows (b) are values for Strike 1 (see Figs 8–11).

possibility is that trochanteral extension is not carried out by direct muscle action. However, the action of TTrE across two articulations allows another possibility. Thus, all remotor torque about the P–C articulation has been assumed to be generated by TTrE activity, this assumption providing the means of determining the relative contributions of TTrE and CTrE to the C–T extensor torque. However, it would be quite possible for the relative contribution of TTrE to the C–T torque to be higher than calculated by this assumption, provided that the CP stress was increased such that the net P–C remotor torque remained unchanged. In Table 4 CTrE muscle output parameters for Strike 1 are recalculated assuming maximum CTrE power output of $450\,W\,kg^{-1}$, whence it can be seen that the involvement of CP and TTrE in trochanteral extension would be sufficient to reduce the calculated power outputs of CTrE to around or below the instantaneous power output values found for other muscles.

The strain rate of CTrE at peak power output is $8{\cdot}4\,s^{-1}$. If the muscle is assumed to be producing nearly maximal power output, this figure implies an intrinsic strain rate in the region of $28\,s^{-1}$. Hence CTrE may be producing significantly less than maximal power output at this time. Table 4 also gives recalculated figures assuming either a maximum power output of $225\,W\,kg^{-1}$ or zero power.

The calculated TTrE stresses rise very rapidly in Fig. 9, and the CP stress curve has a very complex stepped appearance. The evidence is thus strong that the initial method of calculating the performance of the muscles acting about the P–C and C–T articulations underestimates the activity of CP and TTrE and overestimates the activity of CTrE. It seems likely that CTrE stress falls off more quickly than

Table 4. *Peak values of muscle output parameters recalculated assuming restricted values for peak CTrE power output during Strike 1*

Recalculated for reduced maximum power in CTrE ($W kg^{-1}$)	Maximum stress ($kN m^{-2}$)	Maximum strain rate (s^{-1})	Maximum power ($W kg^{-1}$)
	Coxal trochanteral extensor		
Not recalculated	87·8	8·38	735·7
450	53·7	8·38	450·0
225	26·9	8·38	225·0
0	0	–	0·0
	Thoracic trochanteral extensor		
Not recalculated	64·2	0·58	37·2
450	140·0	0·58	81·0
225	185·3	0·58	107·5
0	247·8	0·58	143·7
	Coxal promotor		
Not recalculated	0·0	–	0·0
450	48·7	5·77	281·0
225	78·1	5·77	451·0
0	118·3	5·77	683·0

calculated and that TTrE stress rises correspondingly earlier, the latter being associated with an increased level of CP activity during this phase of the strike. (CTrE stress falling more rapidly than calculated would not only result in lower maximum power outputs but also in lower maximum strain rates, as the strain rate rises rapidly during CTrE activity.)

Allowing for CR activity in the later phases of the strike would also result in smoother and more accurate stress/time curves, though this allowance would not significantly affect the peak calculated values.

Errors introduced by smoothing data

Whilst smoothing techniques are essential when calculating d^2x/dt^2 from noisy values of x, the possibilities of under- or over-smoothing cannot be avoided. These can lead to over- or underestimated peak values of accelerations, which would in turn lead to inaccuracies in stress and power output figures (the small component of high frequency noise seen in some of the calculated stress and power curves is probably due to residual unsmoothed errors in position measurement). Fig. 10 illustrates the effects of different levels of smoothing upon data from these experiments. The importance of smoothing is well illustrated by this plot. Since a smooth acceleration curve is to be expected during normal leg movements, the graphs support the use of nine-point smoothing. The nine-point technique measures accelerations accurately for sine waves with periods of 18 t (where t is the unit time interval between points) and over. Fig. 10 shows that coxal x-acceleration performs slightly under a full sine wave cycle in 14 t during the strike illustrated. Thus, the main acceleration components should be at worst only slightly underestimated, though faster transients of acceleration could be missed. Angular velocities have also been smoothed. However, as only a single

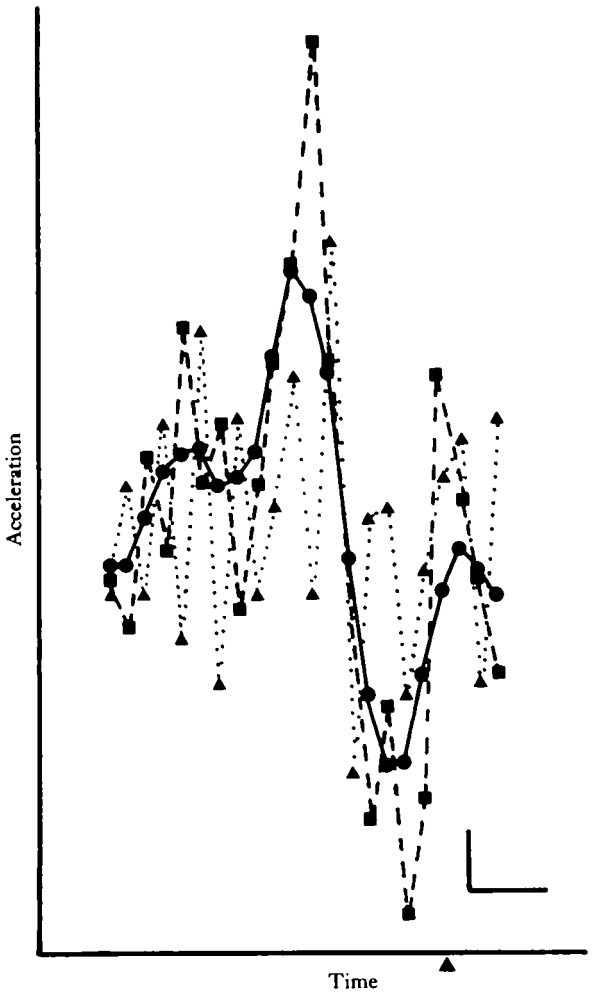

Fig. 10. The effects of different types of smoothing upon the calculation of coxal x acceleration. Circles, solid line – nine-point smoothing (Lanczos, 1957); squares, dashed line – five-point smoothing (Lanczos, 1957); triangles, dotted line – no smoothing. Arrow marks the time at which contact was made with the prey. Vertical bar represents $10\,m^2\,s^{-1}$ (circles, squares), $50\,m^2\,s^{-1}$ (triangles). Horizontal bar represents 10 ms.

differentiation is involved, less smoothing is required, and hence introduced errors will be smaller.

Estimation of frictional effects

The distance s travelled in time t by a body of mass m falling from rest under gravitational force and retarded by a force f_1, is

$$s = \tfrac{1}{2}(g - f_1/m)t^2,$$

therefore:

$$f_1 = mg - 2ms/t^2$$

Consider the system shown in Fig. 11B. A light, balanced bar (the arm of a transducer) is loaded by a mass m at a distance $l_1/5$ from the pivot (where l_1 is the distance from the pivot to the tip). When released the tip of the bar travels a distance s in time t. Hence the mean acceleration of m is given by:

$$a_1 = 2s/5t_1^2,$$

provided that the angular movement of the bar is small so that the vertical is almost tangential. The acceleration a_1 will be less than $\boldsymbol{g}$ due to the force required to produce angular acceleration of the bar and to resistive forces, collectively termed f_1, which will be assumed to be constant throughout the movement.

If the tip of a limb podomere of length l_2 is now attached by a fine thread to the tip of the transducer arm (Fig. 11A), the time taken for the tip of the arm to travel distance s will now be t_2 ($t_2 > t_1$ because of the additional force, f_2, required to accelerate the limb). Hence the mean acceleration of the podomere is given by:

$$a_2 = 2s/5t_2^2$$

and

$$\begin{aligned} f_2 &= 1/5\ (m\boldsymbol{g} - ma_2 - f_1) \\ &= m/5\ (a_1 - a_2) \end{aligned}$$

provided f_1 remains constant.

Since the podomere must be in dynamic equilibrium with the forces acting upon it, the torque produced about the articulation by the gravitational force upon the centre of mass ($m_2\boldsymbol{g}$) and f_2 should be equal to the inertial torque. If any resistive forces act this will result in an inequality. Hence the resistive torque

$$T_r = f_2 l_3 + m_2 \boldsymbol{g} l_2/2 - I_j\dot{\omega},$$

where l_3 is the distance from the articulation to the thread attachment, $l_2/2$ the distance from the centre of mass to the articulation, I_j the moment of inertia of the podomere about the articulation and $\dot{\omega}$ the angular acceleration. Assuming the femur to be a homogeneous rod of length l_2, then

$$I_j = 4/3\ (l_2/2)^2 m_2$$

by the parallel axes theorem. $\dot{\omega}$ was calculated as:

$$\dot{\omega} = 2\,\theta/t^2,$$

where θ is the angle moved by the joint in time t. f_1 will not remain constant as the acceleration of m_1 changes from a_1 to a_2 as it is made up of components which are velocity dependent (e.g. viscous drag) and acceleration dependent (inertial torque of the transducer arm). Hence the resistive torques have been calculated assuming both that f_1 was constant (T_r) and that f_1 was directly proportional to acceleration (T_r^*)

$$(\text{i.e. } f_1^* = f_1\, a_2/a_1),$$

T_r was $2{\cdot}2 \times 10^{-6}$ N m ($\pm 1{\cdot}3$ S.E.M., $N = 7$) and T_r^* was $8{\cdot}6 \times 10^{-6}$ N m ($\pm 3{\cdot}4$ S.E.M., $N = 7$). The true figure should lie within the range of these values.

A further possible error is introduced by the assumption that f_1 is constant during

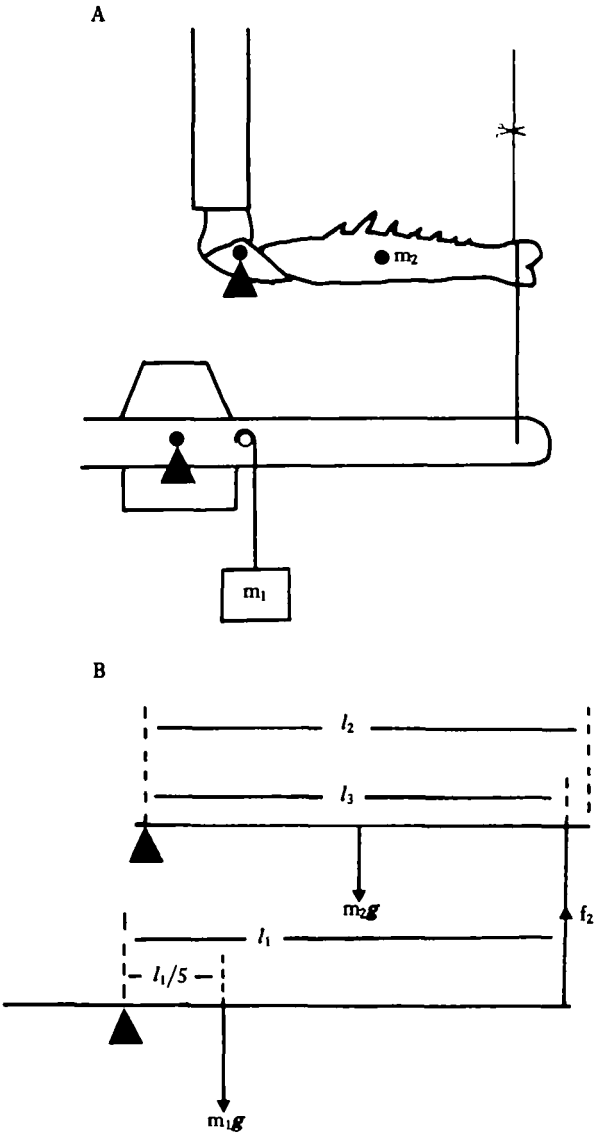

Fig. 11. The method used for the estimation of forces resisting trochanteral extension. (A) The experimental set-up and (B) a mechanical diagram of the set-up. The arrows represent the coxo–trochanteral (C–T) articulation and the transducer pivot. m_1 is the load, m_2 the femoral mass, l_1 the transducer lever arm, l_2 the total femoral length and l_3 the distance from the C–T articulation to the attachment of the line joining the femur and transducer.

a single run whereas f_1 is partly velocity-dependent. The extent of the resulting deviations was examined by comparing mid-point velocities ($V_{0\cdot5}$) with terminal velocities (V_T). The velocities were measured as the tangent to the distance time records. If the acceleration is constant then $V_{0\cdot5}/V_T = 0\cdot5$. The mean observed ratio was 0·56 (0·02 S.E.M., $N = 5$); hence the deviation from constant acceleration is small.

There is considerable spread in the results from these experiments. The standard error of T_r^* is nearly 50 % of the mean value. Peak power output from CTrE occurred

when the C–T torque was in the range $1–2 \times 10^{-4}$ N m and the angular velocity was 20–57 rad s^{-1} in the five strikes analysed. The mean resistive torque in the experiments outlined above was 8×10^{-6} N m and the mean angular velocity 17 rad s^{-1}. Assuming the worst case and using T_r^*, if the resistive torque is assumed to be directly proportional to angular velocity and is adjusted for the C–T angular velocity at peak CTrE power output for each strike, the resistance torques represent 10–14 % of the calculated C–T torque at maximum CTrE power output for the five strikes analysed.

A-band lengths

A-band lengths (Table 5) were used rather than sarcomere lengths as the former remain constant at all muscle lengths, except possibly at extreme contraction.

The A-bands of TiF_{PAR} (2·2 μm) are considerably shorter than those of TiF_{PEN} (3·9 μm), and this fits well with the high contraction rates of TiF_{PAR} and the idea that TiF_{PEN} is adapted for developing high isometric tensions when holding prey. The locust tibial extensor muscle, which is also specialized to produce high isometric stresses, has an A-band length of 5·5 μm (Cochrane, Elder & Usherwood, 1972) and can develop a stress of about 750 kN m^{-2} (Bennet-Clark, 1975). By interpolation, TiF_{PEN} may be expected to be capable of generating 500–600 kN m^{-2}.

The TTrE (2·5 μm) and CTrE (3·8 μm) A-band lengths do not seem to be related to muscle function during the strike as the former undergoes relatively slow, high stress contractions compared with the latter. The function of this arrangement is unclear.

Apodeme cross-sectional areas

The mean cross-sectional areas of six tibial flexor apodemes was 0·084 (±S.E. 0·006) mm^2 and that of six trochanteral flexor apodemes was 0·042 (±S.E. 0·004) mm^2. The mean coxal and femoral lengths of the forelegs from which these apodemes were taken as 19·3 (±S.E. 0·49) mm and 19·6 (±S.E. 0·53) mm respectively, while the overall lengths of those from which the muscle dimensions were taken were 18·3 (±S.E. 0·28) mm and 18·8 (±S.E. 0·32) mm respectively. Scaling accordingly, the mean cross-sectional areas of the tibial flexor and trochanteral extensor apodemes of the legs in which the muscles were measured should have been 0·076 mm^2 and 0·039 mm^2 respectively. If TiF_{PAR} and TiF_{PEN} can produce maximum stresses of 400 kN m^{-2} and 600 kN m^{-2} respectively, the maximum force produced by the whole flexor muscle, using the data of Table 2 will be 5·2 N. Hence the maximum stress on the tibial flexor apodeme will be $6·8 \times 10^7$ N m^{-2}. Assuming the same maximum stress

Table 5. *Muscle A-band lengths*

Muscle	Mean A-band length (μm)	Standard deviation ($N = 9$)
Tibial extensor	3·8	0·13
Tibial $flexor_{PAR}$	2·2	0·08
Tibial $flexor_{PEN}$	3·9	0·08
Coxal trochanteral extensor	3·8	0·14
Thoracic trochanteral extensor	2·5	0·10
Coxal promotor	3·4	0·16

values for TTrE and CTrE as for TiF_{PAR} and TiF_{PEN} respectively, the maximum stress on the trochanteral apodeme will be $6{\cdot}6 \times 10^7\ N\ m^{-2}$. Bennet-Clark (1975) found that the ultimate tensile strength of the locust metathoracic tibial extensor apodeme was about $6{\cdot}0 \times 10^8\ N\ m^{-2}$, and therefore the safety factor for these two apodemes is probably about 10.

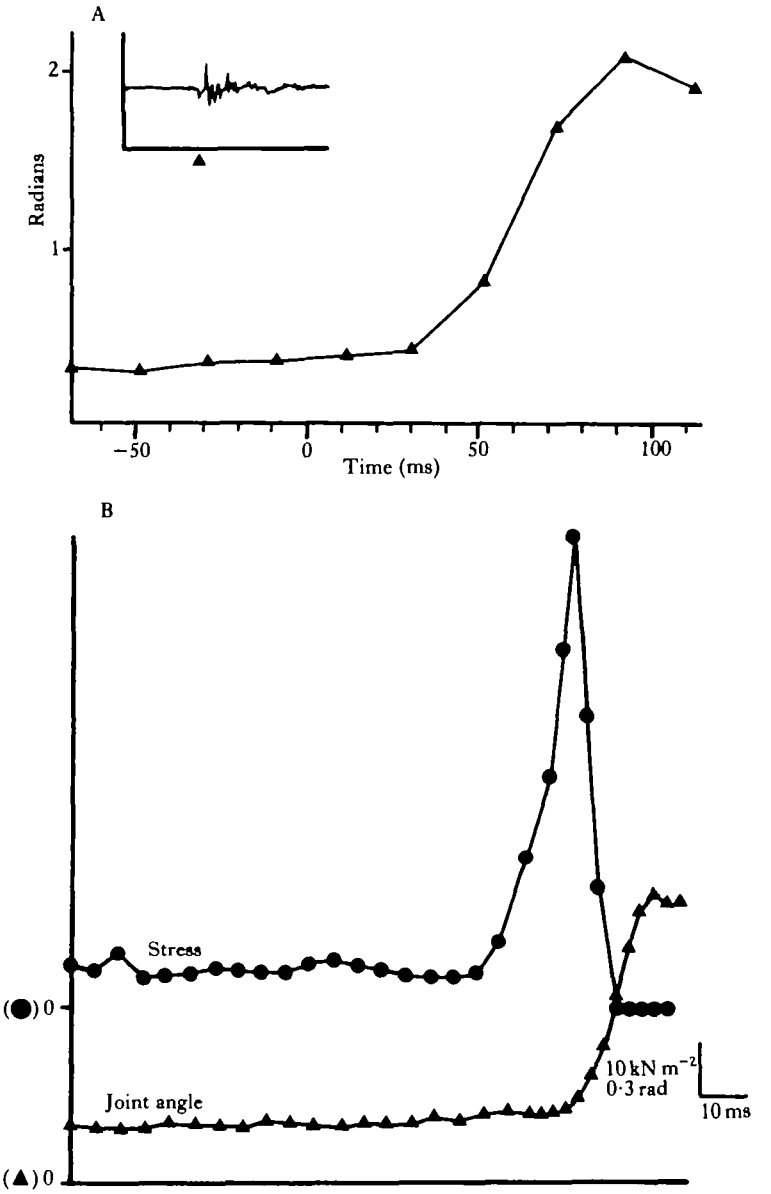

Fig. 12. (A) Relationship between coxal trochanteral EMG and trochanteral extension. The main figure shows C–T angle of articulation plotted against time. The inset is an EMG recorded from implanted, paired copper wire electrodes. The time marks are at 10 ms intervals. The arrow marks the point taken as the onset of EMG activity; this is also taken as zero time in the main figure. (B) Relationship between trochanteral extension and calculated CTrE stress, using a different strike from (A). A delay of about 20 ms between the onset of extensor stress and the start of extension can be seen.

Phasing of muscle activity

The phasing of recorded electrical activity in CTrE to observed trochanteral extension is shown in Fig. 12. The observed delay was 10–30 ms in the five strikes. Fig. 12 shows a delay of 10–20 ms between the rise in calculated CTrE tension and the onset of trochanteral extension. In mouse skeletal muscle, stress development does not occur until 4·3 ms after the start of electrical excitation (Buchtal & Sten-Knudsen, 1959); in insect muscle, delays of 3–7 ms have been observed (Usherwood, 1962; Stokes, Josephson & Price, 1975). There is thus at most a few milliseconds delay between the observed onset of electrical activity in CTrE and that predicted by a model of direct muscle action.

Problems with crosstalk prevented precise determination of the phasing of activity of the various forelimb muscles involved in the strike. However, it is clear from simultaneous EMGs of these muscles that, with the exception of CP, long periods of activity preceding visible movement are not seen prior to the strike in the mantid. In some preparations low levels of activity were observed in CP for considerable periods prior to the strike.

Tibial flexor strain rates

The strain rate of the whole tibial flexor muscle was measured over ranges of moment of 0·4–1·0 mm in response to a single stimulus (2–4 V, 0·1 ms duration) to the main leg nerve, 5. The photodiode was positioned to allow some space (about 0·2 mm) for acceleration before recording started; thus the distances quoted above do not reflect the total length of contraction in response to a single twitch. The muscle was loaded during these experiments with a 1 g mass, as this was necessary to keep the wire carrying the transducer flag taut. As the peak force that this muscle can produce can be estimated to be about 120 g (see above), the recorded strain rates should approach the intrinsic strain rate. The mean strain rate from nine sets of trials, each set from a different leg, was 15·3 ($\pm$S.E. 0·86) s^{-1} assuming a mean TiF_{PAR} fibre length of 10·2 mm (Table 2). The assumption has been made that the observed fast twitch is due to TiF_{PAR} with no involvement of TiF_{PEN} ; for these rates of contraction, strain rates in TiF_{PEN} would approach 40 s^{-1}.

DISCUSSION

With the exception of the tibial flexor muscle, for which very high strain rates were obtained, the calculated peak values of stress, strain rate and power output lie within the range observed in muscles from other animals (Table 1). The peak calculated strain rates for CTrE are also high (14·6 s^{-1}) but, as discussed earlier, the method of calculation of CTrE activity probably overestimates the activity of the muscle in the later stages of trochanteral extension and hence overestimates peak strain rates as the trochanter is accelerating at this time.

On the basis of these results there is no need to postulate a power amplification system of the type observed, for example, in the jumps of the locust (Bennet-Clark, 1975), in the prey capture of mantid shrimps (Burrows, 1969) or in the snapping of

alpheid shrimps (Ritzmann, 1974). However, these results were calculated from the observed movement of the forelimb and thus represent the minimum values of stress, strain rate and power output required to produce the action seen. If there were significant forces involved other than those due to the muscles producing the movement – such as internal or external drag effects, or tension in antagonists (either residual or due to complex patterns of motor activity), then real power outputs could be significantly underestimated.

Measurements of resistive forces involved in trochanteral extension (the highest calculated power requirement for the strike is for trochanteral extension) show that resistive torques represent no more than 14% of the extensor torque at peak power output. This agrees with the finding of Bennet-Clark (1975), from observations of the damped oscillation of the tibia of the locust, that when the jump impulse was released with the leg unloaded, the energy losses from resistive forces during the locust jump were 3–12%. While this level of resistive losses is not insignificant, it is insufficient to require reconsideration of the idea that trochanteral extension in the mantid occurs by direct muscle action.

Electrophysiological measurements indicate that strong activity in the trochanteral extensor starts at most a few milliseconds before the time predicted by a direct action model and there are no lengthy periods of activity in other muscles prior to the strike, with the exception of CP. In the locust jump (Heitler & Burrows, 1977) and mantis shrimp strike (Burrows, 1969) muscle activation occurs 300–1000 ms before the movement.

EMG activity from CP was generally observed to start 0–10 ms before that in CTrE, though low level activity was occasionally seen up to several hundred milliseconds before the onset of activity in CTrE. Corrette (1980) observed a similar pattern of EMG activity associated with the strike in the mantid *Tenodera aridifola*. He noted the close phasing of muscle activity to movement in all muscles except for CP. He regularly recorded variable periods (often exceeding 200 ms) of activity in CP preceding the strike; these were accompanied by small levels of activity in the remotor. Corrette suggested that this could indicate the involvement of a power amplification mechanism in coxal promotion. However, the present study has shown that CP does not produce the highest power output of all the leg muscles, as was assumed by Corrette, and that the required power output for direct muscle action is within the limits observed in muscles from other animals. Furthermore, the EMG activity recorded in CP prior to the strike in both *T. aridifola* and *H. membranacea* was highly variable in both duration and magnitude, though the level of activity was always significantly smaller than during the strike itself. In *Heirodula membranacea*, apparently normal and successful strikes were observed in which no EMG activity in CP was recorded prior to movement. This suggests that, if there is a power amplification mechanism, it is operating at low efficiency (since the muscle is never fully activated before the movement starts) and that it is not essential for successful strikes. No comparative analysis has been carried out of strikes in which prior CP activity was present and absent, so it is impossible to rule out the possibility of some increment in speed resulting from this.

Another possible explanation for the early activity in CP is that the onset of coxal promotion is of long duration, and highly variable. In some strikes slow partial coxal

promotions preceding the strike proper by several hundred milliseconds are observed. Corrette (1980) showed that both the position of the coxa prior to the strike and the degree of coxal promotion during the strike are correlated with the position of the prey. This suggests that coxal position is highly controlled in the lead up to, and is important to the success of, the strike. Thus, these slow movements of the coxa can be interpreted as part of the orientation process preceding the strike. The role of the low levels of CR activity observed by Corrette may be to enhance the stability and precision of these movements, in a similar fashion to the actions of the antagonists in some human finger and thumb movements (eg: MacConaill & Basmajian, 1969).

The strain rates of TiF_{PAR} are of considerable significance. The mean peak value of $17{\cdot}5\ s^{-1}$ at 27–30 °C calculated from ciné analysis of the strike approaches the fastest observed in mammalian muscles operating at 37 °C. As the Q_{10} of muscle strain rates is around 2 [2·67, 2–12 °C, frog muscles (Edman, 1979); 1·68, 25–35 °C, rat E.D.L. (Close, 1972)] this represents an extremely high value. This raised the possibility of fast tibial flexion during the strike being driven by energy stored during extension. However, the observation of high strain rates in *in vitro* stimulated tibial flexor muscles suggests that flexion does in fact occur by direct action. The peak rates ($15{\cdot}3\ s^{-1}$) were slightly smaller than the calculated value discussed above. These values, however, are mean rates for contraction over 0·5–1·0 mm in response to a single stimulus, whereas values calculated from strike analysis represent instantaneous peak values.

The ultrastructure of TiF_{PAR} shows an expected adaptation to high strain rates. The A bands are 2·2 μm long, only slightly longer than those of vertebrates (1·6 μm) and amongst the shortest seen in arthropods (Mill & Lowe, 1971). TiF_{PAR} is, then, well adapted to its role in the strike and an interesting question raised is whether this muscle shows any biochemical specializations relating to its ability to contract nearly as fast as the fastest mammalian muscles at 27–30 °C, temperatures almost 10 °C lower than mammalian body temperature.

The analysis of the strike also illustrates the functional advantages of having one of the coxal extensor muscles originating in the prothorax. The muscle thus operates on two articulations, having an extensor moment arm about the coxo–trochanteral articulation and a remotor moment arm about the prothoracic–coxal articulation. This means that during the strike, since the coxa is undergoing promotion at the time of trochanteral extension, TTrE is able to exert large extensor forces at low strain rate. In effect, in the intermediate stages of the strike (after the principal phases of coxal acceleration have occurred) power is transmitted from the coxal promotor into trochanteral extension directly and also indirectly, since the deceleration of the coxa during trochanteral extension represents transfer of kinetic energy of coxal promotion (previously generated by CP) into trochanteral extension. If TTrE were inserted in the coxa, the power output required of it to produce strikes as observed would be prohibitively high, because in the later stages of the strike the trochanter accelerates, leading to high strain rates, while the stress remains high. As discussed earlier, CTrE is unlikely to make any contribution to the later stages of trochanteral extension – it could not provide significant stress at the strain rates required.

Ultrastructurally, TTrE does not show the specialization that might be expected from the role described above. A muscle exerting large forces at small strain rates

would optimally have long A-bands. However, the A-bands of TTrE are only 2·5 μm long, whereas CTrE, which has high strain rates during the strike, ha[illegible] A-bands 3·8 μm long. The reason for this is unclear but may lie in the role of TTrE in other activities such as walking. An examination of the function and ultrastructure of the thoracic trochanteral extensors of the mid- and hindlimbs of the mantid and of the legs of related species such as the cockroach could throw light upon this question.

The forelimbs of the mantid are able not only to move fast during the strike but also through considerable angles of articulation. As is shown clearly in Fig. 2 a simple single-point attachment to the apodeme cannot provide a workable moment arm throughout the range of movement. The two-point suspension found at four of the apodeme attachments is clearly of great significance in allowing the extensive active movements which the forelimbs perform during prey capture. Such multiple apodeme suspensions have not been described previously but, since many insect limbs have wide freedom of movement and the specialization was observed on four apodemes in the mantid forelimb, it may well occur elsewhere. If this is so it is a finding of some significance to mechanical studies of insect limbs as failure to take account of such complexities of apodeme suspension where they occur could result in inaccurate estimates of moment arms.

In conclusion, although the mantid strike does not make use of a catapult-like power amplification mechanism as observed elsewhere, the forelimb is well specialized to produce a fast strike. Peak power output approached the maximum found in other animals, and several muscles show strain rates that are high in the league for insect muscle, in particular TiF_{PAR} with a peak strain rate significantly higher than those previously observed in arthropods.

That the strike occurs by direct muscle action can be seen as an advantage to the praying mantids as this allows full control over the destination of the strike until the last possible moment (though clearly there is no time for visual feedback during the later stages of the strike). Any form of prior energy storage must introduce an element of stereotyping which is not advantageous to a predator striking moving prey. Furthermore, no speed advantage is secured as prey using fast escape responses based on elastic energy stores must first load them before movement; this is a relatively lengthy process, around 500 ms for a locust. If the mantid maintains the element of surprise, a direct muscle action mechanism should always be fast enough. The mantid shrimp which does make use of a catapult like system has to cope with a heavy calcified exoskeleton, the higher drag of water, its own reactive acceleration (as it is not fixed to the substrate) and furthermore often uses its forelimbs to smash the hard exoskeletons of prey and not just to catch them.

We should like to thank Professor R. McN. Alexander for his advice and also for his valuable comments at the manuscript stage. In addition one of the authors (PTAG) would like to thank the SERC for a research studentship, during the course of which this work was carried out.

REFERENCES

ALEXANDER, R. McN. (1968). *Animal Mechanics*. London: Sidgwick & Jackson.

ALEXANDER, R. McN. (1974). The mechanics of jumping by a dog (*Canis familiaris*). *J. Zool. Lond.* **173**, 549–573.

BENNET-CLARK, H. C. (1975). The energetics of the jump of the locust *Schistocerca gregaria*. *J. exp. Biol.* **63**, 53–83.

BENNET-CLARK, H. C. (1977). Scale effects in jumping animals. In *Scale Effects in Animal Locomotion*, (ed T. J. Pedley), pp. 185–202. London: Academic Press.

BENNET-CLARK, H. C. & LUCEY, E. C. A. (1967). The jump of the flea: a study of the energetics and model of the mechanism. *J. exp. Biol.* **47**, 59–76.

BUCHTAL, F. & STEN-KNUDSEN, O. (1959). Impulse propagation in striated muscle fibres and the role of the internal currents in activation. *Ann. N.Y. Acad. Sci.* **81**, 422–445.

BURROWS, M. (1969). The mechanics and neural control of the prey capture strike in the Mantid shrimps *Squilla* and *Hemisquilla*. *Z. vergl. Physiol.* **62**, 361–381.

CLOSE, R. J. (1972). Dynamic properties of mammalian skeletal muscles. *Physiol. Rev.* **52**, 129–197.

COCHRANE, P., ELDER, H. & USHERWOOD, P. (1972). Physiology and ultrastructure of phasic and tonic skeletal muscle fibres in the locust, *Schistocerca gregaria*. *J. Cell. Sci.* **10**, 419–441.

COPELAND, J. (1975). Coordination of prey capture movement in the Praying Mantis *Tenodera sinensis* with special reference to the lunge. Ph.D. dissertation, S.U.N.Y., Stony Brook, N.Y.

CORRETTE, B. J. (1980). Motor control of prey capture in the Praying mantis, *Tenodera aridifola sinensis*. PhD thesis. University of Oregon, Eugene, Oregon, U.S.A.

EDMAN, K. A. P. (1979). The velocity of unloaded shortening and its relation to sarcomere length and isometric force in vertebrate muscle fibres. *J. Physiol., Lond.* **291**, 143–159.

EVANS, M. E. G. (1972). The jump of the click beetle (Coleoptera: Elateridae) – a preliminary study. *J. Zool., Lond.* **167**, 319–336.

EVANS, M. E. G. (1973). The jump of the click beetle (Coleoptera: Elateridae) – energetics and mechanics. *J. Zool., Lond.* **169**, 181–194.

FRANK, M. E. (1930). An observation on the diet of the Praying Mantis. *J. Linn. Soc. (Zool.)* **9**, 321–322.

GRAY, P. (1954). *The Microtomists Formulary and Guide*. London: Constable.

GRAY, P. T. A. (1981). Structural and physiological aspects of prey capture in the praying mantis *Heirodula membranacea*. Ph.D. thesis. University of Leeds, Leeds, U.K.

HEITLER, W. J. & BURROWS, M. (1977). The locust jump. I. The motor programme. *J. exp. Biol.* **66**, 203–219.

KER, R. (1977). Some mechanical and structural properties of locust and beetle cuticle. Ph.D. thesis. Oxford University, Oxford, U.K.

LANCZOS, C. (1957). *Applied Analysis*. London: Pitman.

MACCONAILL, M. A. & BASMAJIAN, J. V. (1969). *Muscles and Movements*. Baltimore: Wilkins & Wilkins.

MALDONADO, H., LEVIN, L. & BARROS-PITA, J. C. (1967). Hit distance and the predatory strike of the praying mantis. *Z. vergl. Physiol.* **56**, 237–257.

MENDELSON, M. (1969). Properties of a very fast lobster muscle. *J. Cell Biol.* **42**, 548–563.

MENDEZ, J. & KEYS, A. (1960). Density and composition of mammalian muscles. *Metabolism* **9**, 184–188.

MILL, P. J. & LOWE, D. A. (1971). Ultrastructure of the respiratory and non-respiratory dorso-ventral muscles of the larva of a dragonfly. *J. Insect Physiol.* **17**, 1947–1960.

MITTLESTAEDT, H. (1954). Regelund und Steuerung bei der Orientierung der Lebewesen. *Regelungastechnik* **2**, 226–232.

MITTLESTAEDT, H. (1957). Prey capture in mantids. In *Recent Advances in Invertebrate Physiology*, (ed B. T. Scheer). Oregon: University of Oregon.

PENNYCUICK, C. J. & PARKER, G. A. (1966). Structural limitations on the power output of the pigeons flight muscles. *J. exp. Biol.* **45**, 489–498.

PROSSER, C. L. (1973). Muscles. In *Comparative Animal Physiology*, (ed. C. L. Prosser), pp. 719–798. Philadelphia: Saunders.

RITZMANN, R. E. (1974). Mechanism for the snapping behaviour of the alpheid shrimp, *Alpheus heterchelis*. *J. comp. Physiol.* **95**, 217–236.

ROEDER, K. D. (1959). A physiological approach to the relation between prey and predator. *Smithson. misc. Collns* **137**, 287–306.

STOKES, D. R., JOSEPHSON, R. K. & PRICE, R. B. (1975). Structural and functional heterogeneity in an insect muscle. *J. exp. Zool.* **194**, 379–408.

USHERWOOD, P. N. R. (1962). The nature of 'slow' and 'fast' contractions in the coxal muscles of the cockroach. *J. Insect Physiol.* **7**, 31–52.

WEIS-FOGH, T. (1956). Tetanic force and shortening in locust flight muscle. *J. exp. Biol.* **33**, 668–684.

WEIS-FOGH, T. & ALEXANDER, R. MCN. (1977). The sustained power output from striated muscle. In *Scale Effects in Animal Locomotion*, (ed. T. J. Pedley), pp. 511–525. London: Academic Press.